frontiers in Materials

ORIGINAL RESEARCH
published: 09 March 2021
doi: 10.3389/fmats.2021.638733

NiCo Nanorod Array Supported on Copper Foam as a High-Performance Catalyst for Hydrogen Production From Ammonia Borane

Liling Li[1], Binshan Guo[2], Hang Li[2], Xibin Zhang[2], Yufa Feng[2] and Jinyun Liao[2]**

[1]Department of Pharmacy, Huizhou Health Sciences Polytechnic, Huizhou, China, [2]School of Chemistry and Materials Engineering, Guangdong Provincial Key Laboratory for Electronic Functional Materials and Devices, Huizhou University, Huizhou, China

Searching for inexpensive, durable, and active catalysts for the dehydrogenation of ammonia borane (AB) is an important subject in the field of hydrogen energy. In this study, we have fabricated NiCo nanorod arrays anchored on copper foam (CF) by a simple hydrothermal process. The catalytic performance of those array catalysts in AB hydrolysis was studied. It was found that NiCo-1/CF showed the highest catalytic activity with a hydrogen generation rate (HGR) of 1.03 $L_{hydrogen}$ g^{-1} min^{-1}, which was much higher than that for the unsupported NiCo-1 catalyst. It has been demonstrated that strong base can significantly enhance hydrogen production. After six catalytic cycles, the morphology, crystal structure, and catalytic activity were maintained, indicating that the NiCo-1/CF sample showed good reusability and high durability. Considering their low cost and high performance, the NiCo nanorod arrays anchored on CF can be a strong candidate catalyst for hydrogen generation for mobile hydrogen-oxygen fuel cells.

Keywords: hydrogen production, ammonia borane, heterogeneous catalysis, nanorods, NiCo alloys

OPEN ACCESS

Edited by:
Zhenhai Xia,
University of North Texas, United States

Reviewed by:
Bao Yu Xia,
Huazhong University of Science and Technology, China
Zhenmeng Peng,
University of Akron, United States

****Correspondence:***
Yufa Feng
yufafeng@126.com
Jinyun Liao
jyliao@126.com

Specialty section:
This article was submitted to Energy Materials, a section of the journal Frontiers in Materials

Received: *07 December 2020*
Accepted: *25 January 2021*
Published: *09 March 2021*

Citation:
Li L, Guo B, Li H, Zhang X, Feng Y and Liao J (2021) NiCo Nanorod Array Supported on Copper Foam as a High-Performance Catalyst for Hydrogen Production From Ammonia Borane. Front. Mater. 8:638733. doi: 10.3389/fmats.2021.638733

INTRODUCTION

The traditional carbon-based energy system is regarded as the main source of environmental pollution, which brings great challenges to the sustainable development of our society. It is an important task to look for "green energy," which can be applied at an industrial scale. Possessing the merits of high calorific value, renewable nature, and zero emissions, hydrogen is considered as an ideal substitute for carbon-based fossil fuels (Cipriani et al., 2014; Uyar and Beşkci, 2017; Hirscher et al., 2019). Before the large-scale application of hydrogen, hydrogen must be efficiently produced, stored, and transported safely. It is well established that storage is the bottleneck of applications of hydrogen energy (Ren et al., 2017; Abe et al., 2019). A number of methods have been developed to address the bottleneck issue. Among them, hydrogen storage via chemical hydride is attractive because of its safety and high efficiency (Wang et al., 2019; Zhou et al., 2019). In addition, when hydrogen is stored in chemical hydrides, hydrogen storage and production can be integrated into one step, which can remarkably reduce the processing costs. For example, ammonia borane (AB) is a typical chemical hydride. It is very stable in the form of both aqueous and solid states, so it can be easily and safely transported. As for the production of hydrogen, AB can release hydrogen in the form of an aqueous state by a catalytic process (Feng et al., 2021; Akbayrak and Özkar, 2018). In 2006, Xu's group first demonstrated that Pt, Ru, and Pd catalysts can effectively catalyze AB hydrolysis (Chandra and Xu, 2006). Among them, Pt exhibited the highest catalytic activity. After that,

heterogeneous catalysts have attracted much attention in this field. Although noble metal-based catalysts are active for AB hydrolysis, the high costs impede wide applicability in the industry (Zhong et al., 2016; Fu et al., 2018). Thus, a number of cheap nonnoble metal-based heterogeneous catalysts have been developed, which are expected to replace those expensive catalysts in practical applications. Among the inexpensive catalysts, Co-based and Ni-based nanocatalysts exhibit relatively high catalytic activity in AB hydrolysis (Rakap and Özkar, 2010; Wang et al., 2016; Tang et al., 2017). For example, Figen et al. prepared an amorphous Co-B catalyst by a sol-gel reaction and carried out catalytic hydrolysis of AB under ultrasonic conditions (Figen and Coşkuner, 2013). They found the hydrogen generation rate (HGR) was 0.9152 $L_{hydrogen}\ g^{-1}\ min^{-1}$. Shan et al. fabricated a series of Ni_3B/C catalysts and tested their catalytic activity in AB hydrolysis. It was discovered that HGR for Ni_3B/C catalysts was 1.168 $L_{hydrogen}\ g^{-1}\ min^{-1}$ (Shan et al., 2014). Zhou et al. supported Ni nanoparticles of an average size of *ca.* 10 nm on carbon materials and demonstrated that the HGR for Ni/C in AB hydrolysis is 0.83 $L_{hydrogen}\ g^{-1}\ min^{-1}$ (Zhou et al., 2014). Very recently, Yang et al. synthesized Ni-Fe-P catalysts, which exhibit a HGR of 0.7 $L_{hydrogen}\ g^{-1}\ min^{-1}$ (Yang et al., 2019). Over the past several years, significant progress has been made on the unsupported and supported Co-based and Ni-based catalysts. As for the supported catalysts toward AB hydrolysis, there are two groups of commonly used substrates. The first group is the powdery substrates on the macro-level, such as activated carbon, carbon nanotubes, graphene, and SiO_2 microspheres. The second group is the film substrate, such as Ti sheet, Cu foam, and Ni foil. Generally speaking, when the first group of substrates were used, the nanocatalysts anchored on the substrates are always spherical particles. It is difficult to control the morphology of those nanocatalysts. On the contrary, when the second group of substrates were used, anisotropic crystal growth of nanocatalysts on the substrates could happen. For example, nanosheets, nanorod, and nanowires supported on the surface of the film substrate have been widely reported (Liao et al., 2019b). It is well known that the morphology of the nanocatalysts may significantly affect their activity. In general, those anisotropic nanocrystals, such as nanosheets and nanorods, will exhibit much improved catalytic activity in contrast to the spherical counterparts because they possess much more edges, corners, and faces, which are always active sites for catalytic reactions (Shan et al., 2014; Yan et al., 2016). In addition, it is very simple to collect and recover those film catalysts from the reaction medium. Thus, the overall cost of the catalytic process in practical applications can be remarkably reduced.

Considering these factors together, it is believed that a Co/Ni-based film catalyst composed of nanocatalysts with well-controlled morphology will exhibit superior catalytic performance compared to their powdery counterparts and provide great potential in practical applications. However, to the best of our knowledge, nanostructured CoNi alloy film has been seldom reported, especially applications in the catalytic hydrolysis of AB. In this study, NiCo alloy nanostructures anchored on the surface of copper foam (CF) film were prepared by a simple one-step process. CF is used as a substrate on account of its low cost and high stability. The molar ratio of Ni to Co was tuned to achieve a high catalytic activity. It is interesting to note that NiCo nanorods supported on CF show high activity with a HGR of 1.03 $L_{hydrogen}\ g^{-1}\ min^{-1}$ in AB hydrolysis.

EXPERIMENTAL

Synthesis

All chemical reagents were obtained from commercial suppliers and used without further purification. In a typical synthesis, $NiCl_2{\cdot}6H_2O$ and $CoCl_2{\cdot}6H_2O$ with the total amount of 4 mmol were added to a beaker containing 20 ml water, followed by the addition of disodium ethylene diamine tetraacetate (4.5 mmol) with stirring. Then, NaOH solution (1.25 M, 20 ml) was added dropwise to the above suspension and a transparent solution was obtained. After that, 10 ml ethanol was poured into a mixture solution. The resultant solution was transferred into a Teflon-lined autoclave (100 ml), in which a piece of CF with a size of 5 × 12 cm was attached to the inner wall of the Teflon cup. After hydrazine hydrate solution (50 wt.%, 10 ml) was added to the Teflon cup, the autoclave was sealed and heated at 150°C for 4 h. After reacting, the CF and powder precipitated at the bottom of the reaction vessel were collected, washed, and dried. To prepare NiCo alloys with different molar ratios, the initial molar ratios of $NiCl_2{\cdot}6H_2O$ to $CoCl_2{\cdot}6H_2O$ were set as 1:3, 2:2, and 3:1, respectively. Correspondingly, the samples supported on CF were named NiCo-1/CF, NiCo-2/CF, and NiCo-3/CF, respectively. The corresponding powdery samples were named NiCo-1, NiCo-2, and NiCo-3, respectively.

Characterizations

A Rigaku D/Max-1200X diffractometer with Cu Kα radiation was applied to record the X-ray powder diffraction (XRD) patterns of the samples. A Hitachi Su-8010 field emission scanning electron microscope (FE-SEM) was used to analyze the morphology of the samples. Elemental mapping analysis was carried out using an EDAX Octane Elite energy disperse spectrometer (EDS) coupled with FE-SEM. The element ratios of Co:Ni of different samples were measured using an Agilent 7,800 inductively coupled plasma-mass spectrometer (ICP-MS).

Catalytic Experiments

In a typical experiment, a film catalyst (5 × 3 cm) was suspended into 10.0 ml water under ultrasonication. Then, 10 ml mixed solution of AB (0.3 M) and NaOH (2 M) was added to the vessel, which was sealed and connected to a glass burette. After the mixture, the final NaOH concentration is 1.0 M. The reaction vessel was immersed into a water bath at a temperature of 298 K. The volume of the produced hydrogen was determined by recording the displacement of water in the gas burette. To study the stability and reusability of our catalyst, the catalytic experiments were repeated six times. When the previous run finished, 3 mmol of AB was added to the remaining reaction

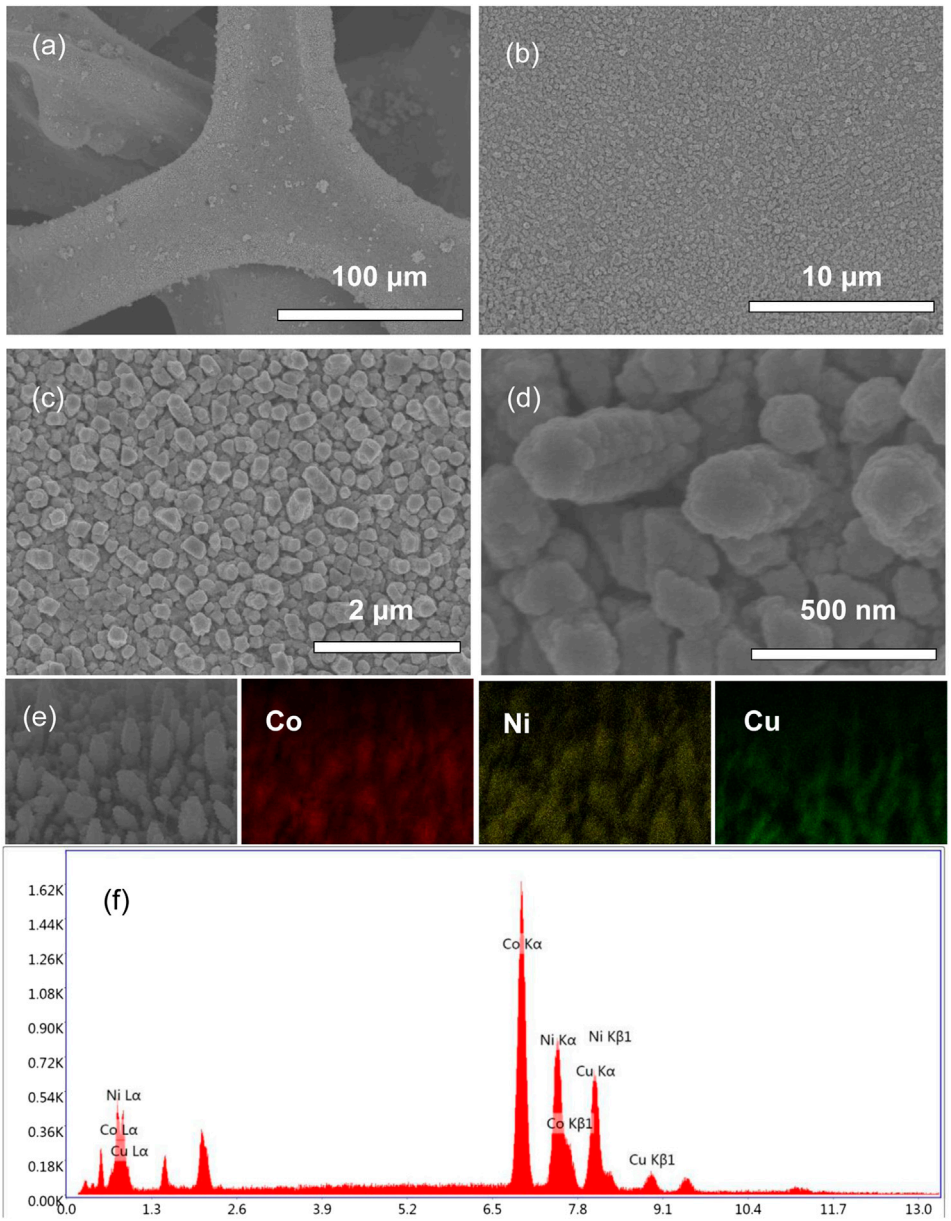

FIGURE 1 | SEM images at different magnifications **(A–D)**, elemental mapping **(E)**, and EDS pattern **(F)** of NiCo-1/CF.

solution containing catalyst and a new run began. The hydrogen volume was monitored during different catalytic runs, and the stability and reusability of the catalyst were assessed.

RESULTS AND DISCUSSION

Figure 1 shows the SEM images of NiCo-1/CF. As can be seen, the surface of CF after NiCo deposition looks very uniform (**Figures 1A,B**). The magnified SEM image reveals the surface is rather coarse and filled with many nanorods (**Figure 1C**). These nanorods are vertical to the CF surface, which looks like a nanorod array. **Figure 1D** indicates that the typical nanorod diameter is approximately 200 nm. Elemental mappings in **Figure 1E** demonstrate that Ni and Co are uniformly distributed on the CF surface, implying that Co and Ni are

TABLE 1 | The molar ratios and deposited NiCo mass of three samples.

Samples	Molar ratio of Ni to Co determined by ICP-MS	[a]Deposited NiCo mass (mg)
NiCo-1/CF	0.38:1	136.7
NiCo-2/CF	1.12:1	147.0
NiCo-3/CF	2.85:1	190.8

[a]*This value was calculated by the difference of CF mass after and before NiCo deposition.*

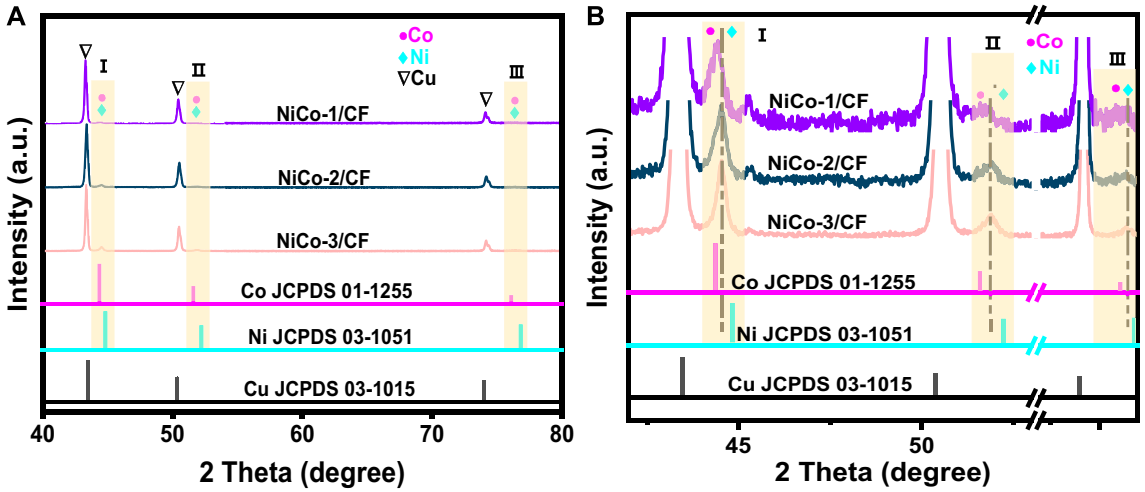

FIGURE 2 | XRD patterns **(A)** and magnified XRD patterns **(B)** of NiCo-1/CF, NiCo-1/CF, and NiCo-1/CF.

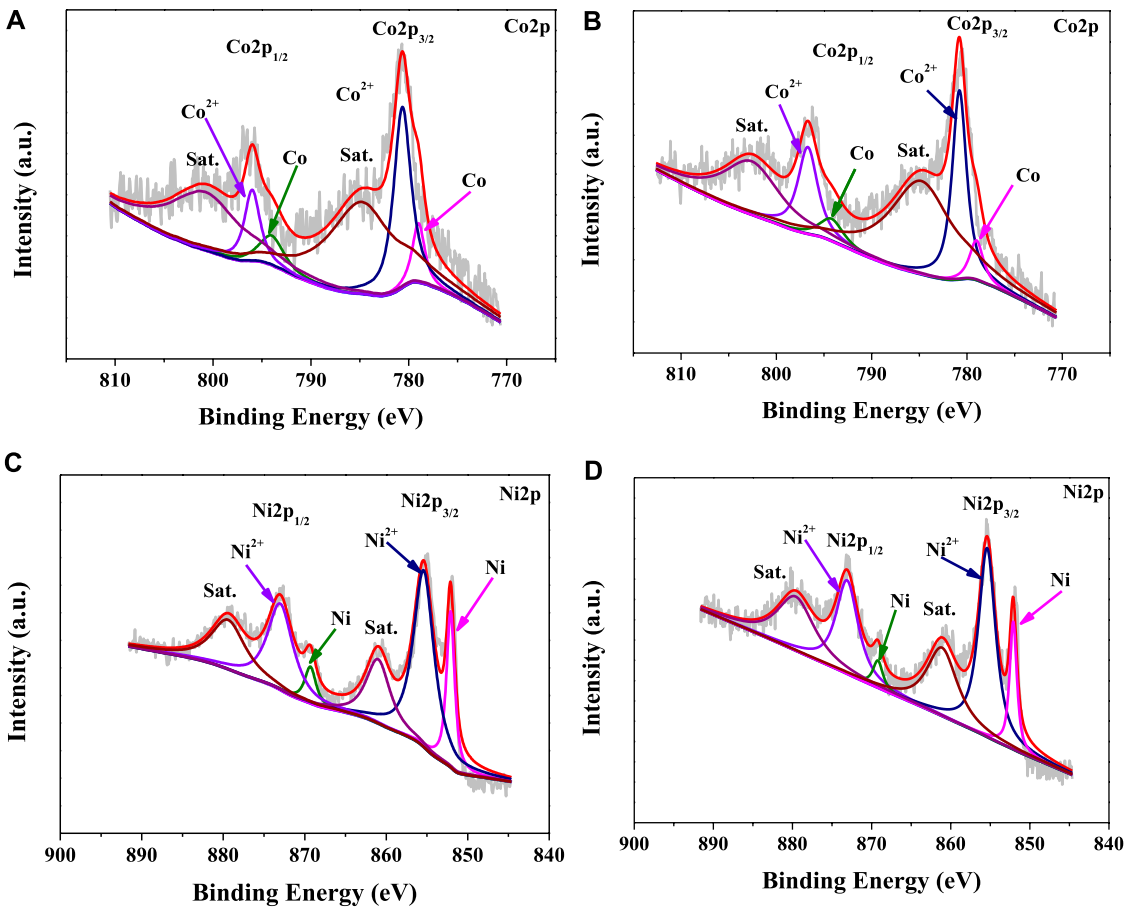

FIGURE 3 | XPS spectra in the Co 2p and Cu 2p regions of the NiCo-1/CF samples before **(A,C)** and after **(B,D)** catalytic reactions.

presented as alloys rather than solo metals. The EDS pattern of NiCo-1/CF in **Figure 1F** indicates that elements of Co and Ni, as well as Cu, are observed. For comparison, the morphologies of NiCo-2/CF and NiCo-3/CF were also investigated by SEM. **Supplementary Figure S1** shows that both NiCo-2/CF and NiCo-3/CF have similar morphologies to NiCo-1/CF. To know

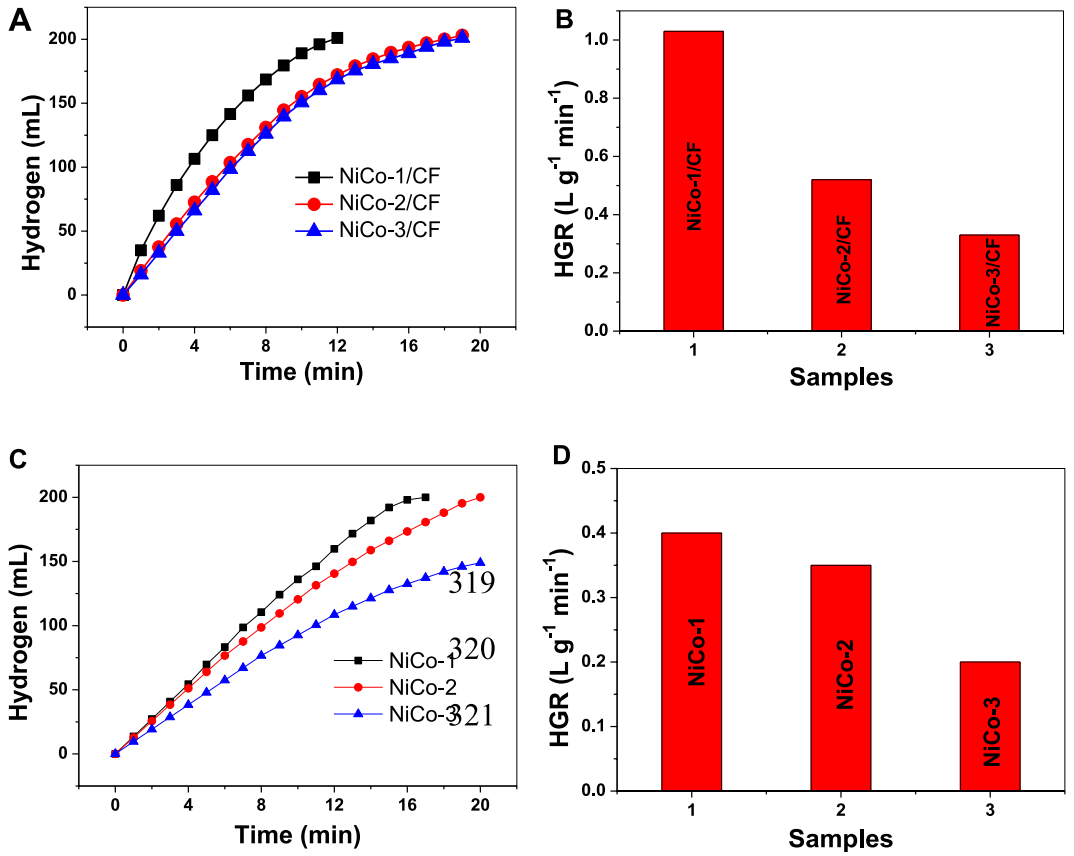

FIGURE 4 | Hydrogen evolution **(A,C)** and corresponding HGR values **(B,D)** for CF-supported NiCo samples and unsupported NiCo samples.

more about the different samples, information about the molar ratio and deposited NiCo mass of the three samples is shown in **Table 1**. It is interesting to note that the deposited NiCo mass will increase as the Co/Ni ratio decreases. It is possible that it is easier for Ni to anchor on CF surface.

Figure 2A shows the XRD patterns of NiCo-1/CF, NiCo-2/CF, and NiCo-3/CF and the standard pattern of metallic Cu, Ni, and Co. The characteristic peaks of Cu can be clearly observed in the three samples. However, the peaks related to Co and Ni are weak and can hardly be observed. In the magnified XRD patterns in **Figure 2B**, three peaks appear at $2\theta = 44.3^{\circ}$, 51.6°, and 76.2° besides the characteristic peaks of Cu. When comparing these three peaks with those in the standard patterns of metallic Co and Ni, it is evident that these three peaks are related to Co and Ni. Notably, the peaks marked with I, II, and III lie between the corresponding peaks of Co and Ni, implying that the materials supported on CF are NiCo alloys rather than metallic Ni and Co (Liao et al., 2019), which match the elemental mapping results.

Figure 3 shows the XPS spectra of the NiCo-1/CF in the Co 2p and Cu 2p regions. As shown in **Figure 3A**, the Co $2p_{3/2}$ peak can be deconvoluted into two peaks at 780.6 and 779.0 eV, while the Co $2p_{1/2}$ peak can be deconvoluted into two peaks at 786.0 and 794.1 eV. The first and third peaks are attributed to the Co^{2+}, and the second and fourth peaks are ascribed to metallic Co (Zhang et al., 2019). Similarly, the Ni $2p_{3/2}$ peak can be deconvoluted into two peaks at 855.4 and 852.1 eV, while the Ni $2p_{1/2}$ peak can be deconvoluted into two peaks at 873.1 and 869.3 eV (**Figure 3C**). The first and third peaks are attributed to the Ni^{2+} and the second and fourth peaks are ascribed to metallic Ni (Zhu et al., 2018). Notably, the oxidation states of Co and Ni are detected on the surface of the sample by XPS. However, no characteristic peaks of CoO and NiO are observed in the XRD pattern of the sample. These findings indicate that partial oxidation of Co and Ni on the surface of NiCo-1/CF occurs. This is understandable because nanosized NiCo alloys are liable to be oxidized on their surface when they are exposed to the air. However, the trace surface oxides cannot arouse diffraction in the XRD pattern. Similar results have also been reported by other groups who have found that Co^{2+} and Ni^{2+} coexist with Co(0) and Ni(0) on the surface of nanostructured CoNi alloys (Cheng et al., 2019; Zhang et al., 2019).

The catalytic activities of different samples were investigated, and the results are displayed in **Figure 4A**. In a preliminary experiment, it was found that no hydrogen was produced in the presence of bare CF, indicating that CF substrates have no catalytic activity to AB hydrolysis. In contrast, after NiCo was deposited on the surface of CF, they possessed good catalytic activity to AB hydrolysis. Evidently, the catalytic activity is attributed to the NiCo alloy rather than the CF substrate. It should be mentioned that the NiCo masses in different samples were not the same. To properly assess the catalytic activity of different samples, the NiCo mass

should be taken into consideration. According to the literature, the catalytic activity of a catalyst in AB hydrolysis can be evaluated in terms of HGR, which is the volume of generated hydrogen per minute and per gram of catalyst. **Figure 4B** shows the HGR of different NiCo/CF samples for comparison. HGR values for NiCo-1/CF, NiCo-2/CF, and NiCo-3/CF were 1.03, 0.52, and 0.33 $L_{hydrogen}\ g^{-1}\ min^{-1}$, respectively. Evidently, NiCo-1/CF possesses higher catalytic activity than the other two samples. Many factors will affect the catalytic performance of heterogeneous nanocatalysts, such as morphology, components, and surface states. In this study, three samples were synthesized at similar conditions and their morphologies were similar. Thus, it is likely that their activity difference is related to the molar ratios of Co to Ni. According to previous reports, NiCo alloys have higher catalytic activity than solo Ni and Co metals in AB hydrolysis due to the synergistic effects between Ni and Co. However, it seems that there are no consistent results in the literature regarding optimized molar ratios of Co to Ni of the catalysts for AB hydrolysis. For example, Co_xNi_{1-x}/XC-72 developed by Wang et al. exhibited the highest catalytic activity in AB hydrolysis when the molar ratio of Co to Ni is 0.6 to 0.4 (Wang et al., 2017). Feng et al. have found that Co_xNi_{1-x} nanoparticles supported on graphene achieve the best catalytic performance in the case of Co/Ni ratio of 0.9 to 0.1 (Feng et al., 2014). However, Miao et al. discovered that a relatively low Co/Ni ratio in CoNi alloy resulted in better catalytic activity, who demonstrated that Co_1Ni_1 shows the highest catalytic activity in AB hydrolysis among Co_1Ni_1, Co_1Ni_2, Co_1Ni_3, and Co_1Ni_4 catalysts (Miao et al., 2019). Regarding our developed catalysts, the highest catalytic performance was achieved at a Co/Ni ratio of 1:0.38. Further investigation is needed for a detailed explanation.

In this study, unsupported NiCo catalysts were also prepared and their similar morphologies can be observed in **Supplementary Figure S2**. For comparison, the hydrogen evolution and HGR in the presence of the unsupported catalysts, namely, NiCo-1, NiCo-2 and NiCo-3, were also shown in **Figures 4C,D**. It should be mentioned that the mass of NiCo in the powdery sample equals that in the corresponding film sample. The HGR values for NiCo-1, NiCo-2, and NiCo-3 are 0.40, 0.35, and 0.20 $L_{hydrogen}\ g^{-1}\ min^{-1}$, respectively, which are significantly lower than the corresponding values for the film samples. When NiCo catalysts are presented as powder, NiCo tends to aggregate together under magnetic attraction to each other, which lowers the numbers of active catalytic sites. In this case, the catalytic activity will decrease. However, when NiCo is anchored on the surface of CF, aggregation of NiCo catalysts will not occur. Thus, the catalytic activity loss associated with the catalyst aggregation can be avoided. So, the NiCo/CF samples exhibit much improved catalytic activity compared to the corresponding powdery NiCo samples. To assess catalytic activity, the HGR value of our NiCo-1/CF (1.03 $L_{hydrogen}\ g^{-1}\ min^{-1}$) was compared with those of some Co-based and Ni-based catalysts reported by other groups. It was higher than the HGR of the amorphous Co-B catalyst (0.9152 $L_{hydrogen}\ g^{-1}\ min^{-1}$) (Figen and Coşkuner, 2013), Ni/C catalysts (0.83 $L_{hydrogen}\ g^{-1}\ min^{-1}$) (Zhou et al., 2014), Fe-Ni nanoparticles on polyethyleneimine-decorated graphene oxide (0.982 $L_{hydrogen}\ g^{-1}\ min^{-1}$) (Zhou et al., 2012), 3D porous Ni-Zn catalyst (0.52 $L_{hydrogen}\ g^{-1}\ min^{-1}$) (Wei et al., 2019), and Ni-Fe-P catalysts (0.7 $L_{hydrogen}\ g^{-1}\ min^{-1}$) (Yang et al., 2019). However, it is still lower than the HGR of Ni_3B/C catalysts (1.168 $L_{hydrogen}\ g^{-1}\ min^{-1}$) (Shan et al., 2014) and Co-B-P catalysts (1.25 $L_{hydrogen}\ g^{-1}\ min^{-1}$) (Fernandes et al., 2013). Anyway, our NiCo-1/CF exhibits a relatively high catalytic activity. There are two possible reasons for the high catalytic activity of the NiCo-1/CF catalyst. The first one is related to the synergistic effects between Ni and Co. According to Cheng et al., when Ni is incorporated into Co, the d-band of the obtained NiCo alloy will downshift and the energy barrier of the rate-determining step in AB hydrolysis for NiCo alloy catalyst will decrease compared with those of Ni and Co (Cheng et al., 2019). In that case, their activity will be remarkably enhanced. The second one may be attributed to the nanorod morphology of the catalysts. It is widely reported that those anisotropic nanocrystals, such as nanosheets and nanorods, will exhibit much improved catalytic activity in contrast to the spherical nanoparticles because they possess much more edges, corners, and faces, which are always active sites for catalytic reactions (Li and Shen, 2014; Yan et al., 2016).

In this work, it is found that NaOH concentration in the reaction medium can remarkably affect the HGR. This is very important in practical applications because the HGRs can be controlled to some degree by simply adjusting the NaOH concentration. As seen in **Figure 5A**, in the absence of NaOH, the hydrogen production rate is rather slow. Evidently, NaOH can significantly promote the hydrolysis reaction. The hydrolysis of ammonia borane is as follows:

$$H_3NBH_3\,(aq) + 2H_2O\,(l) \rightarrow NH_4^+ + (aq) + BO_2^-\,(aq) + 3H_2\,(g).$$

In the presence of NaOH, it is clear that NH_4^+ will be consumed by OH^-, which can help shift the chemical equilibrium to the right. Thus, AB hydrolysis is enhanced. When NaOH concentration increases to 0.5 M, the HGR increases to 0.65 $L_{hydrogen}\ g^{-1}\ min^{-1}$. When NaOH concentration increases to 1.0 M, the HGR increases further to 1.03 $L_{hydrogen}\ g^{-1}\ min^{-1}$ (**Figure 5B**). Notably, HGR at a NaOH concentration of 1.5 M is close to that at NaOH concentration of 1.0 M, suggesting that an excessive amount of NaOH is unfavorable for AB hydrolysis. The viscosity of the reaction medium will become higher with higher concentrations of NaOH introduced into the reaction solution (Liao et al., 2019b). It is well known that the viscosity of the reaction medium has a great impact on the migration rate of the reactants to the catalyst surface. In a medium with high viscosity, it is possible that the motion of AB to NiCo-1/CF surface slowed and the internal diffusion rate of the reaction was lowered. In this case, a NaOH concentration that is too high will not result in increased HGR.

The dependence of HGR on the hydrolysis temperature on AB hydrolysis catalyzed by NiCo-1/CF was investigated in the temperature range from 293 to 318 K. As shown in **Figure 6A**, it is clear that HGR increased very quickly with increasing temperature. When the temperature increased from 293 to 318 K, the completion time for the hydrolysis reaction at 318 K is about 40% of the time experienced at 293 K. The Arrhenius equation, namely, $\ln k = -E_a/(RT) + \ln A$, was applied to calculate the apparent activity energy (E_a) of AB hydrolysis catalyzed by NiCo-1/CF, in which k is the rate constant of hydrolysis reaction, R the molar gas constant, T

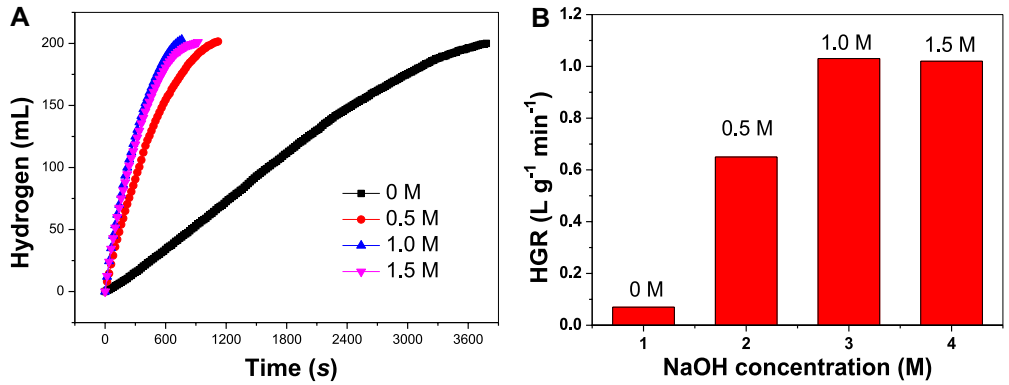

FIGURE 5 | (A) Hydrogen evolution in the presence of different NaOH concentrations and **(B)** the corresponding HGR values.

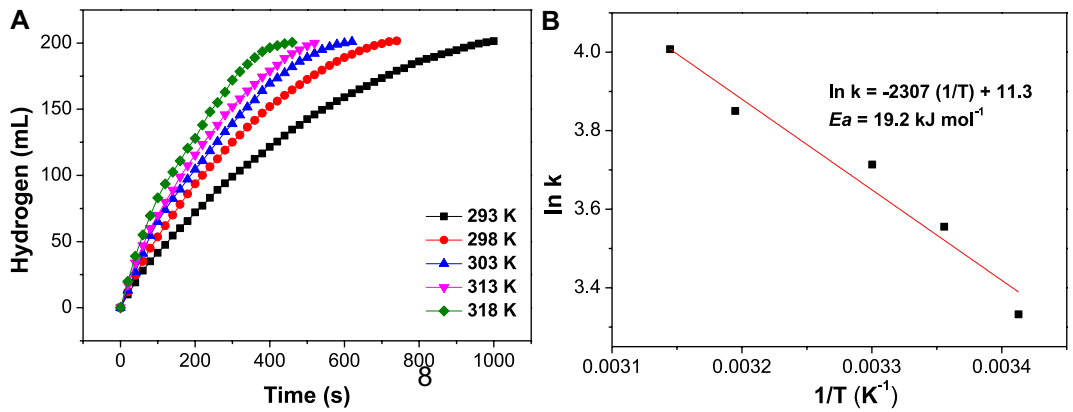

FIGURE 6 | Effects of reaction temperatures on hydrogen evolution when NiCo-1/CF acts as a catalyst **(A)** and its corresponding Arrhenius plot **(B)**.

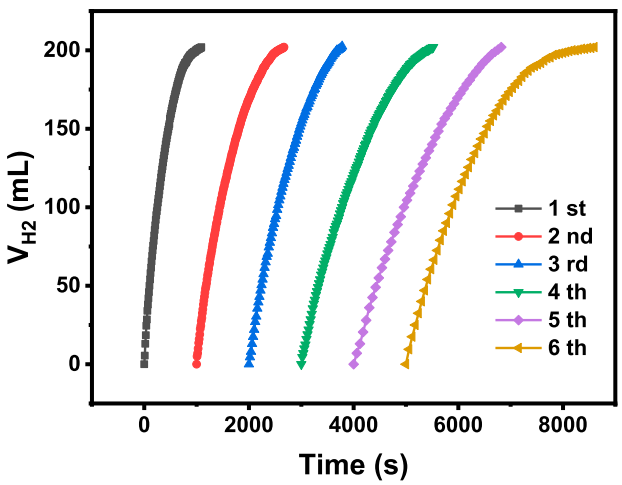

FIGURE 7 | Hydrogen evolution at different catalytic cycles when NiCo-1/CF acts as a catalyst.

the reaction temperature (K), and A the preexponential factor. According to the Arrhenius equation, E_a of AB hydrolysis in the presence of NiCo-1/CF as a catalyst was calculated to be 19.2 kJ/mol (**Figure 6B**). E_a is one of the lowest values among the Co-based or Ni-based catalysts reported in the literature (Wang et al., 2020a; Wang et al., 2020b).

In practical applications, the durability and reusability of a catalyst are crucial factors that determine its real cost. **Figure 7** shows the hydrogen evolution at different catalytic cycles in the presence of NiCo-1/CF as a catalyst. As the cycle number increases, only a slight decrease in hydrolysis rate was observed. It should be mentioned that BO^- will be produced during AB hydrolysis, which may be adsorbed on the catalyst surface and occupy the active sites (Rakap and Özkar, 2010). As described in the experimental section, our catalyst was not refreshed by removing the adsorbed BO^- after each catalytic run. Thus, it is understandable that activity slightly decreased. Notably, even at the sixth run, the hydrogen volume generated during catalytic hydrolysis is more than 200 ml, demonstrating a full conversion of AB to hydrogen. This demonstrates that our

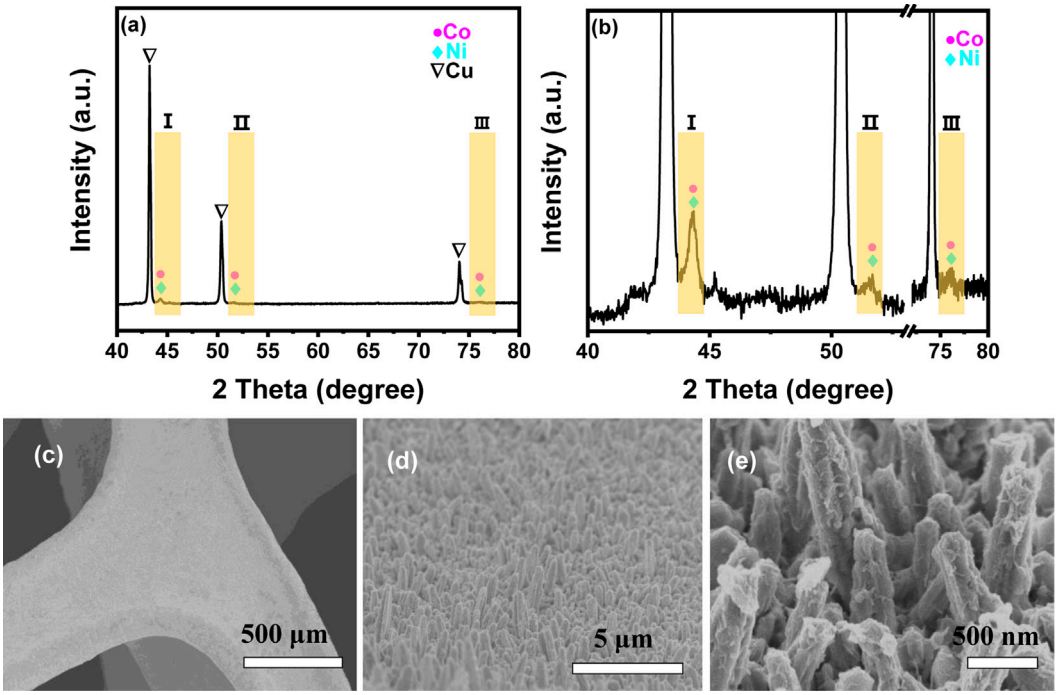

FIGURE 8 | XRD pattern **(A)**, magnified XRD pattern **(B)**, and SEM images **(C–E)** of NiCo-1/CF after catalytic reaction.

sample shows good reusability and high durability in AB hydrolysis. We have checked the used NiCo-1/CF sample with SEM, XRD, and XPS. **Figure 8**, **Figures 3B,D** show that there are no remarkable changes in the morphology, crystal structures, and the chemical states on the surface of NiCo-1/CF after catalysis, further verifying the good reusability and high durability of our sample.

CONCLUSION

In summary, we have fabricated CF-supported NiCo nanorod arrays by a simple hydrothermal process. The samples were characterized with XRD, SEM, and EDS. It was found that NiCo-1/CF showed the highest catalytic activity in AB hydrolysis with a HGR of 1.03 $L_{hydrogen}\ g^{-1}\ min^{-1}$, which was much higher than that for the unsupported NiCo-1 catalyst. It has been demonstrated that NaOH can remarkably improve hydrogen production. After six catalytic cycles, the morphology, crystal structures, and catalytic activity were maintained, verifying the NiCo-1/CF sample shows good reusability and high durability. Considering their low cost and high performance, the NiCo nanorod arrays anchored on CF can be strong candidate catalysts for hydrogen generation for mobile hydrogen-oxygen fuel cells.

DATA AVAILABILITY STATEMENT

The raw data supporting the conclusions of this article will be made available by the authors without undue reservation.

AUTHOR CONTRIBUTIONS

LL was involved in the synthesis of the sample and writing—original draft preparation; BG and HL were involved in the investigation of the catalytic performance; HL and XZ were involved in the characterization and analysis of the sample; YF and JL were involved in the supervision, funding acquisition, and writing—review and editing. All authors have given their approval to the final version of the manuscript.

FUNDING

This work was supported by the Major Project of Fundamental and Application Research of the Department of Education of Guangdong Province (No. 2017KZDXM079), the Natural Science Foundation of Guangdong Province (No. 2018A030313859), the Major and Special Project in the Field of Intelligent Manufacturing of the Universities in Guangdong Province (No. 2020ZDZX2067), and the Natural Science Foundation of Huizhou University (Nos. 20180927172750326).

SUPPLEMENTARY MATERIAL

The Supplementary Material for this article can be found online at: https://www.frontiersin.org/articles/10.3389/fmats.2021.638733/full#supplementary-material.

REFERENCES

Abe, J. O., Popoola, A. P., Ajenifujia, E., and Popoola, O. M. (2019). Hydrogen energy, economy and storage: review and recommendation. *Int. J. Hydrogen Energ.* 44, 15072–15086. doi:10.1016/j.ijhydene.2019.04.068

Akbayrak, S., and Özkar, S. (2018). Ammonia borane as hydrogen storage materials. *Int. J. Hydrogen Energ.* 43, 18592–18606. doi:10.1016/j.ijhydene.2018.02.190

Chandra, M., and Xu, Q. (2006). A high-performance hydrogen generation system: transition metal-catalyzed dissociation and hydrolysis of ammonia-borane. *J. Power Sourc.* 156, 190–194. doi:10.1016/j.jpowsour.2005.05.043

Cheng, S., Liu, Y., Zhao, Y., Zhao, X., Lang, Z., Tan, H., et al. (2019). Superfine CoNi alloy embedded in Al_2O_3 nanosheets for efficient tandem catalytic reduction of nitroaromatic compounds by ammonia borane. *Dalton Trans.* 48, 17499–17506. doi:10.1039/c9dt03838h

Cipriani, G., Dio, V. D., Genduso, F., Cascia, D., Liga, R., Miceli, R., et al. (2014). Perspective on hydrogen energy carrier and its automotive applications. *Int. J. Hydrogen Energ.* 39, 8482–8494. doi:10.1016/j.ijhydene.2014.03.174

Feng, W., Yang, L., Cao, N., Du, C., Dai, H., Luo, W., et al. (2014). *In situ* synthesis of bimetallic CoNi catalysts supported on grapheme for hydrolytic dehydrogenation ammonia borane. *Int. J. Hydrogen Energ.* 39, 3371–3380. doi:10.1016/j.ijhydene.2013.12.113

Fernandes, R., Patel, N., Paris, A., Calliari, L., and Miotello, A. (2013). Improved H_2 production rate by hydrolysis of Ammonia Borane using quaternary alloy catalysts. *Int. J. Hydrogen Energ.* 38, 3313–3322. doi:10.1016/j.ijhydene.2012.12.085

Feng, Y., Chen, X., Wang, H., Li, X., Huang, H., and Liu, Y. (2021). Durable and high performing Ti supported Ni0.4Cu0.6Co2O4 nanoleaf-like array catalysts for hydrogen production. *Renew. Energ.* 169, 660–669. doi:10.1016/j.renene.2021.01.048

Figen, A. K., and Coşkuner, B. (2013). A novel perspective for hydrogen generation from ammonia borane with Co-B catalysts: "Ultrasonic Hydrolysis". *Int. J. Hydrogen Energ.* 38, 2824–2835. doi:10.1016/j.ijhydene.2012.12.067

Fu, F., Wang, C., Wang, Q., Martinez-Villacorta, A., Escobar, A., Chong, H., et al. (2018). Highly selective and sharp volcano-type synergistic Ni_2Pt@ZIF-8-catalyzed hydrogen evolution from ammonia borane hydrolysis. *J. Am. Chem. Soc.* 140, 10034–10042. doi:10.1021/jacs.8b06511

Hirscher, M., Autrey, T., and Orimo, S. (2019). Hydrogen energy. *Chemphyschem* 20, 1157. doi:10.1002/cphc.201900429

Li, Y., and Shen, W. (2014). Morphology-dependent nanocatalysts: rod-shaped oxides. *Chem. Soc. Rev.* 43, 1543–1574. doi:10.1039/c3cs60296f

Liao, J., Feng, Y., Wu, S., Ye, H., Zhang, J., Zhang, X., et al. (2019b). Hexagonal $CuCo_2O_4$ nanoplatelets, a highly active catalyst for the hydrolysis of ammonia borane for hydrogen production. *Nanomaterials* 9 (1–11), 360. doi:10.3390/nano9030360

Liao, J., Lv, F., Feng, Y., Zhong, S., Wu, X., Zhang, X., et al. (2019a). Electromagnetic-field-assisted synthesis of Ni foam film-supported CoCu alloy microspheres composed of nanosheets: a high performance catalyst for the hydrolysis of ammonia borane. *Catal. Commun.* 122, 16–19. doi:10.1016/j.catcom.2019.01.010

Miao, H., Ma, K., Zhu, H., Yin, K., Zhang, Y., and Cui, Y. (2019). Ammonia borane dehydrogenation and selective hydrogenation of functionalized nitroarene over a porous nickel–cobalt bimetallic catalyst. *RSC Adv.* 9, 14580–14585. doi:10.1039/C9RA01551E

Rakap, M., and Özkar, S. (2010). Hydrogen generation from the hydrolysis of ammonia-borane using intrazeolite cobalt (0) nanoclusters catalyst. *Int. J. Hydrogen Energ.* 35, 3341–3346. doi:10.1016/j.ijhydene.2010.01.138

Ren, J., Musyoka, N. M., Langmi, H. W., Mathe, M., and Liao, S. (2017). Current research trends and perspectives on materials-based hydrogen storage solutions: a critical review. *Int. J. Hydrogen Energ.* 42, 289–311. doi:10.1016/j.ijhydene.2016.11.195

Shan, X., Du, J., Cheng, F., Liang, J., and Tao, Z. (2014). Carbon-supported Ni_3B nanoparticles as catalysts for hydrogen generation from hydrolysis of ammonia borane. *Int. J. Hydrogen Energ.* 39, 6987–6994. doi:10.1016/j.ijhydene.2014.02.122

Tang, C., Qu, F. L., Asiri, A. M., Luo, Y. L., and Sun, X. P. (2017). CoP nanoarray: a robust non-noble-metal hydrogen-generating catalyst toward effective hydrolysis of ammonia borane. *Inorg. Chem. Front.* 4, 659–662. doi:10.1039/C6QI00518G

Uyar, T., and Beşkci, D. (2017). Integration of hydrogen energy systems into renewable energy systems for better design of 100% renewable energy communities. *Int. J. Hydrogen Energ.* 42, 2453–2456. doi:10.1016/j.ijhydene.2016.09.086

Wang, C., Li, L., Yu, X., Lu, Z., Zhang, X., Wang, X., et al. (2020a). Regulation of d-band electrons to enhance the activity of Co-based non-noble bimetal catalysts for hydrolysis of ammonia borane. *ACS Sustain. Chem. Eng.* 8, 8256–8266. doi:10.1021/acssuschemeng.0c01475

Wang, L., Rawal, A., and Aguey-Zinsou, K.-F. (2019). Hydrogen storage properties of nanoconfined aluminium hydride (ALH_3). *Chem. Eng. Sci.* 194, 64–70. doi:10.1016/j.ces.2018.02.014

Wang, Q., Zhang, F., Du, F., and Liu, T. (2017). A cost effective cobalt nickel nanoparticles catalyst with exceptional performance for hydrolysis of ammonia-borane. *J. Nanoscience Nanotech.* 17, 9333–9338. doi:10.1166/jnn.2017.14331

Wang, X. P., Liao, J. Y., Li, H., Wang, H., and Wang, R. F. (2016). Solid-state-reaction synthesis of cotton-like CoB alloy at room temperature as a catalyst for hydrogen generation. *J. Colloid. Interf. Sci.* 475, 149–153. doi:10.1016/j.jcis.2016.04.033

Wang, Y., Pan, L., Chen, Y., Shen, G., Wang, L., Zhang, X., et al. (2020b). Mo-doped Ni-based catalyst for remarkably enhancing catalytic hydrogen evolution of hydrogen-storage materials. *Int. J. Hydrogen Energ.* 45, 15560–15570. doi:10.1016/j.ijhydene.2020.04.061

Wei, L., Liu, Q., Liu, S., and Liu, X. (2019). 3D porous Ni-Zn catalyst for catalytic hydrolysis of sodium borohydride and ammonia borane. *Funct. Mater. Lett.* 13 (1–4), 1950093. doi:10.1142/S1793604719500930

Yan, J., Liao, J., Li, H., Wang, H., and Wang, R. (2016). Magnetic field induced synthesis of amorphous CoB alloy nanowires as a highly active catalyst for hydrogen generation from ammonia borane. *Catal. Commun.* 84, 124–128. doi:10.1016/j.catcom.2016.06.019

Yang, J., Yuan, Q., Liu, Y., Huang, X., Qiao, Y., Lu, J., et al. (2019). Low-cost ternary Ni-Fe-P catalysts supported on Ni foam for hydrolysis of ammonia borane. *Inorg. Chem. Front.* 6, 1189–1194. doi:10.1039/c9qi00048h

Zhang, Q., Li, X., Tao, B., Wang, X., Deng, Y., Gu, X., et al. (2019). CoNi based alloy/oxides@N-doped carbon core-shell dendrites as complementary water splitting electrocatalysts with significantly enhanced catalytic efficiency. *Appl. Catal. B-Environ.* 254, 634–646. doi:10.1016/j.apcatb.2019.05.035

Zhong, W. D., Tian, X. K., Yang, C., Zhou, Z. X., Liu, X. W., and Li, Y. (2016). Active 3D Pd/graphene aerogel catalyst for hydrogen generation from the hydrolysis of ammonia-borane. *Int. J. Hydrogen Energ.* 41, 15225–15235. doi:10.1016/j.ijhydene.2016.06.263

Zhou, C., Bowman, R. C., Jr, Fang, Z. Z., Lu, J., Xu, L., Sun, P., et al. (2019). Amorphous TiCu-based additives for improving hydrogen storage properties of magnesium hydride. *ACS Appl. Mater. Inter.* 11, 38868–38879. doi:10.1021/acsami.9b16076

Zhou, L., Zhang, T., Tao, Z., and Chen, J. (2014). Ni nanoparticles supported on carbon as efficient catalysts for the hydrolysis of ammonia borane. *Nano Res.* 7, 774–781. doi:10.1007/s12274-014-0438-7

Zhou, X., Chen, Z., Yan, D., and Lu, H. (2012). Deposition Deposition of Fe–Ni nanoparticles on polyethyleneimine-decorated grapheme oxide and application in catalytic dehydrogenation of ammonia borane. *J. Mater. Chem.* 22, 13506–13516. doi:10.1039/C2JM31000G

Zhu, J., Yin, H., Gong, J., Furjan, M., and Nie, Q. (2018). *In situ* growth of Ni/NiO on N-doped carbon spheres with excellent electrocatalytic performance for non-enzymatic glucose detection. *J. Alloy. Compd.* 748, 145–153. doi:10.1016/j.jallcom.2018.03.125

Conflict of Interest: The authors declare that the research was conducted in the absence of any commercial or financial relationships that could be construed as a potential conflict of interest.